Journal of Molecular Liquids 401 (2024) 124630

Contents lists available at ScienceDirect

Journal of Molecular Liquids

journal homepage: www.elsevier.com/locate/molliq

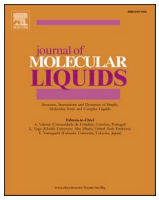

Anomalous behaviour of the ionic conductivity of nanoconfined IL -lithium salt mixtures

P. Vallet [a], J.J. Parajó [a], A. Santiago-Alonso [a,b], M. Villanueva [a], Ó. Cabeza [c], L.M. Varela [a], J. Salgado [a,*]

[a] NAFOMAT Group, Departamentos de Física Aplicada y Física de Partículas, Instituto de Materiales (iMATUS), Universidade de Santiago de Compostela, 15782 Santiago de Compostela, Spain
[b] ABCR Labs Lg. Vilapouca (PG Industrial), 36550 Forcarei (Pontevedra), Spain
[c] MESTURAS Group, Departamento de Física y Ciencias de la Tierra, Universidade da Coruña, 15071 A Coruña, Spain

ARTICLE INFO

Keywords:
Ethylimidazolium nitrate
Quasi-solid electrolytes
Thermal behaviour
Ionic conductivity
Electrochemical devices

ABSTRACT

The effect of salt addition on the protic ionic liquid (IL) ethylimidazolium nitrate is analysed in this work in terms of structural changes measured by NMR, thermal behaviour and ionic conductivity. Additionally, the effect of the immobilization of these mixtures in nano-silica structures on the same properties is also studied. Results show that the influence of salt on the chemical shifts of the signals associated to hydrogen atoms in the apolar regions of the ionic liquid is almost negligible, both in liquid and gel states. The salt accommodates in the polar region of the IL, according to the nanostructured solvation paradigm. The liquid range increases with salt concentration in both states, being this effect especially interesting for high and low temperature applications. The ionic conductivity takes appropriate values to use these compounds as electrolytes in electrochemical devices; pure IL presents 6.9 $mS{\cdot}cm^{-1}$ at 298 K rising to 17.38 $mS{\cdot}cm^{-1}$ at 323 K and this property decreases with salt concentration in the liquid state, as can be expected. Although gel samples present lower ionic conductivity than liquid samples, an anomalous behaviour can be observed in the ionogel samples upon the salt concentration, characterized by an absolute maximum, 13.26 $mS{\cdot}cm^{-1}$ at 323 K, at the lowest salt concentration (0.5 $mol{\cdot}kg^{-1}$ of Li^{+} salt addition), which represents the 12 % higher than the corresponding values of pure ionogel at this temperature.

1. Introduction

Currently, one of the main challenges for the quality of human life future years is the widespread availability of clean, viable and cheap energy. Renewable energy plays a clear and fundamental role in this challenge, although due to its intermittency in production, efficient systems of energy storage are a smart add-on to consider. Consequently, the academy and industry are currently focused on improving performance, safety and cost of battery technology. To achieve these improvements, replacing the currently used flammable electrolytes with non-flammable compounds, as for example ionic liquids (ILs) doped with inorganic salts containing relevant metals for this electrochemical application, is an essential line under continuous study and implementation [1–4].

ILs are nanostructured compounds considered as a new class of green solvents; besides non-flammability, ILs have important properties such as high thermal and chemical stabilities, high ionic conductivity, wide electrochemical window, negligible vapour pressure and, the most relevant, the possibility of tuning their properties by choosing the appropriate combination of cation and anion. All these features have attracted the attention of researchers to be used in lots of applications including electrochemistry [4–8].

The most traditional batteries used aqueous solution electrolytes, although in the last two decades new nonaqueous electrolytes based on organic liquid carbonates solvents with lithium salts are designed, as it is reported by the Nobel Prize J. Goodenough [9] for the development of lithium-ion battery. In addition, in this last decade the number of works concluding the accomplishment of ILs and their mixtures as electrolytes for batteries, supercapacitors, fuel cells, sensors, etc, has exponentially increased [2,4,10–13]. Nevertheless, their liquid state can be a limitation, such for example in packaging, leakage, and portability. The confinement of ILs in nano-scaffolds is proposed as a clever strategy for

* Corresponding author.
E-mail address: j.salgado.carballo@usc.es (J. Salgado).

https://doi.org/10.1016/j.molliq.2024.124630
Received 27 December 2023; Received in revised form 25 March 2024; Accepted 31 March 2024
Available online 1 April 2024

overcoming this problem [14].

The incorporation of ILs into the pore of a porous material leads to the constitution of a new class of hybrid materials, ionogels, with the intrinsic properties of ILs and original functions of a solid matrix [15]. The confinement of a well-stabilized thin layer of IL in a porous matrix may significantly reduce the quantity of IL necessary for a certain application, and then reduces the cost [16].

The most used porous matrices for the confinement of ILs are made, mainly, by silica, TiO_2, SnO_2, porous carbons, and carbon nanotubes [15]. The behaviour and properties of the confined states are dependent of both, IL and matrix precursors. Numerous studies indicate that the confinement tends to reduce the melting temperature, and even suppress phase transitions [2,17–19], although Chen *et al.* [20] found that the confinement of IL in carbon nanotubes causes an increase of more than 200 °C in melting temperature. This indicates that the properties of the ionogel, specifically thermal and transport properties, can be modified significantly by tuning the structure of the confining network [14], but for a detailed understanding of the influence of the network and the IL on these properties, further studies delving into these aspects are needed.

The noteworthy and well-known properties of ILs, particularly their wide electrochemical window and high ionic conductivity, combined with the thermally stable inorganic scaffold, make possible to think in quasi-solid state electrolytes with good electrochemical performances. The duality of the ionogels, created as solids while simultaneously maintaining the macroscopic properties of ILs, leads to more and more electrochemical studies introducing the use of solid-like electrolytes in energy storage devices remarking the enhancement in safety and manipulation [1,2,21]. However, key properties for this application, as the ionic conductivity, after gelation are not yet deeply understood. For instance, Garaga *et al.* [22] found an enhancement on ionic mobility of different ILs (protic and aprotic) confined on nanoporous silica networks, nevertheless, Noor *et al.* [21] found that the conductivity of [BMIm][BF_4] in tetraethoxysilane (TEOS) network is always lower than the bulk IL. These controversial observations suggest that the behaviour of the ionogel can be highly dependent on its synthesis process. Zhang *et al.* [15] highlight the importance of using vacuum in the gelation process, removing the gas accumulated within the pores, so more space for the IL is available inside the network, which affects the transport properties, as Noor *et al.* [21] concluded in their study.

In previous studies [23,24], we reported the effect of monovalent ($LiNO_3$), divalent ($Mg(NO_3)_2$ and $Ca(NO_3)_2$), and trivalent ($Al(NO_3)_3$) salts on several equilibrium and transport properties of mixtures of these salts with protic IL ethylammonium nitrate (EAN). The results showed a decrease in the degree of hydrogen bonding of the PIL with salt concentration and formation of long-lived anionic clusters in the polar regions that act as stable kinetic entities. Additionally, in a recent paper [25] we have found important differences on electrical conductivity of the liquid and silica-gel states of ethylammonium nitrate and $LiNO_3$ mixtures. While this magnitude decreases with salt concentration in liquid samples, it increases at low concentrations of $LiNO_3$ up to a maximum in the gelled samples. This result seems to be associated with the frustration of the formation of solvation complexes due to nanoconfinement.

The initial aim of this work is to enhance the knowledge of these hybrid materials, ILs and their mixtures with salts of electrochemical interest confined in silica scaffolds as potential electrolytes for energy storage devices. Then, changes in thermal behaviour, structural configuration, and ionic conductivity of PIL 1-Ethylimidazolium nitrate as a consequence of the addition of different concentrations of lithium nitrate salt were firstly analysed. Additionally, the effect of the subsequent confinement of these IL + salt mixtures in a silica matrix in previous studied properties was also evaluated.

2. Materials and methods

2.1. Chemicals

The IL used in this work, 1-Ethylimidazolium nitrate ([C_2Im][NO_3]), was purchased from IOLITEC. Solutions of this IL with lithium nitrate salt, provided by Merck, at different concentrations, with molality ranging from 0.5 mol kg^{-1} to 3 mol kg^{-1}, were prepared. Table 1 shows the identification, chemical structure, molecular weight, purity and provenance of chemicals used in this work.

[C_2Im][NO_3] sample was purified via high vacuum for at least 48 h in order to remove water and volatile contents. Values of water content lower than 100 ppm were obtained from Karl Fischer titration after purification. Mixtures were prepared by mixing both components, stirred in a round flask with an ultrasound bath during 24 to 48 h, and were also purified with vacuum during 48 h. The mass of metal salt per 100 g of pure IL for every mixture is indicated in Table 2.

2.2. Gelation route

A sol–gel procedure, adapted from the method described by Garaga *et al.* [22], was carried out to prepare the ionogel samples. The methodology was the following:

a) A mixture of ethanol, TEOS and IL in volume proportions of 3:0.428:1 of EtOH, TEOS and [C_2Im][NO_3] respectively were prepared and stirred in a round flask during 60 min at room temperature.
b) The mixture was transferred to a vial and stored in a furnace at 40 °C until ethanol was completely evaporated (7–8 days) and the gelation was finished.
c) Finally, high vacuum, up to 48 h, was used to eliminate the impurities and complete the ionogel formation.

3. Experimental section

3.1. NMR spectra

Bruker NEO-750 spectrometer of 17.6 T (proton resonance 750 MHz) or DRX-500 spectrometer of 11.7 T (proton resonance 500 MHz) were utilized to obtain NMR spectra at 313.15 K. NEO-750 spectrometer was equipped with a PA-TXI 1H/13C/15 N triple resonance probe, with shielded PFGz-gradient capability. The DRX-500 spectrometer was equipped with a BBI 1H/BB double resonance probe with shielded PFGz-gradient.

NMR samples were prepared in 5 mm standard tubes. An external capillary containing a 5 mM solution of 2,2,3,3-d4-3-(trimethylsilyl)propionic acid (TSP) in Dimethyl Sulfoxide-d6 (DMSO-d_6) was inserted coaxially in the 5 mm NMR tube containing the sample for deuterium lock and external chemical shift reference. The peak of TSP appearing in the ^{1}H and ^{13}C NMR spectra was referenced to $\delta^{1H} = 0$ ppm and $\delta^{13C} = 0$ ppm, respectively [26].

The 1D ^{1}H spectrum was obtained (NEO-750, pulse sequence “zg” of Bruker library) under quantitative conditions using a low excitation tilt pulse angle of only 5 degrees, 64 scans with an inter-scan delay (d1) of 4 s and an acquisition time (aq) of 2.88 s.

The 1D ^{13}C spectrum was obtained (NEO-750 Bruker library) with 256 scans, a relaxation delay (d1) of 2 s and a fid acquisition time (aq) of 0.72 s. The ^{13}C hard pulse was applied with a low tilt angle of 30 degrees. Broad-band 1H decoupling was applied during the relaxation and fid acquisition time periods with a waltz-16 decoupling sequence applied with field strength of 8.33 kHz. The fid was acquired with 64 k complex data points and was processed with zero-filling and FT to obtain a spectrum with 128 k data points.

Table 1
Identification of chemicals used in this work.

Name	Molecular weight (g·mol^{-1})	Structure	CAS number	Provenance	Purity
Ethyl Imidazolium Nitrate	159.14	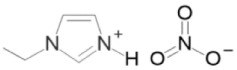	[C_2Im][NO_3] 501693-38-5	Iolitec	>0.98[a]
Lithium Nitrate	68.946	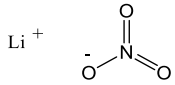	$LiNO_3$ 7790-69-4	Sigma Aldrich	>0.999[a]
Tetraethoxysilane	208.33	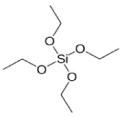	TEOS 78-10-4	Sigma Aldrich	>0.98[a]

[a] Indicated by provider.

Table 2
Molality of the studied samples and mass of pure metal salts per 100 g of pure IL.

Molality /$molt_{salt}$·$kg^{-1}_{[C\ 2Im][NO3]}$	Pure salt mass /g (100 g of IL)$^{-1}$
0.5	3.4486
1.0	6.8973
1.5	10.3459
2.0	13.7945
3.0	20.6918

Standard uncertainty is u (mass) = 0.0001 g and Relative Expanded Uncertainty Ur (molality) = 0.001 (0.95 level of confidence (k = 2)).

3.2. Liquid range

A differential scanning calorimeter (DSC Q1000 TA-Instruments) with hermetically sealed aluminium pans was used to determine the different state transitions experimented by pure IL and salt solutions, in liquid and gel conditions, during heating and cooling cycles under nitrogen atmosphere. All samples were subjected, at least, to four thermal ramps, two in cooling and two in heating mode, with an isothermal step between them:

(a) heating from 25 to 120 °C at 20 °C min^{-1},
(b) isothermal step at 120 °C during 45 min to remove impurities, free water content and to erase the thermal history of the sample [24],
(c) cooling from 120 to −85 °C at 5 °C·min^{-1},
(d) isothermal step at −85 °C during 5 min,
(e) heating from −85 °C to 100 °C at 10 °C·min^{-1},
(f) cooling from 100 °C to −85 °C at 5 °C·min^{-1},
(g) heating from −85 °C to 100 °C at 5 °C·min^{-1}.

Transition temperatures were determined from the DSC curves, as the onset points of the different peaks, during the reheating and recooling steps following the methodology used in previous papers [24,27]. Uncertainties in transition temperatures were estimated as 2 °C at 95 % confidence.

A thermogravimetric analyser (TGA/DTA Mettler Toledo) with simultaneous detection of instantaneous weight and heat flow signals allows a better characterization of mass loss process that takes place in the sample. Dynamic mode under nitrogen atmosphere was used to study the thermal stability of the pure IL and the salt solutions in liquid and gel forms. Samples ranged from 3 to 5 mg were placed in an open platinum pan. Experiments were performed at temperatures from 100 to 800 °C, at 10 °C min^{-1} and with a purge gas flow of 20 cm^3 min^{-1}. Onset temperatures were directly determined from the TGA curves using the methodology described in previous papers [23,24], with the uncertainties of 6 K for onset temperature and 2 % for the mass loss.

3.3. Electrical conductivity

Electrical conductivity (σ) has been measured using a GLP31 CRISON conductimeter, with a resolution better than 1 % of the measured value (with a minimum resolution of 2 × 10^{-6} mS cm^{-1}). All data were measured at least twice in different samples to ensure reproducibility, which was better than 5 % in absolute value. The measuring cells are formed by two parallel plane plates covered with platinum oxide, and were used to measure conductivities in both phases, liquid and solid. The temperature of the samples was controlled using a Julabo thermostat, which provided a precision better than 0.1 K in the temperature range 243 to 323 K. It is important to note that all measurements were done by means of a static isothermal method; thus, the sample was allowed to spend about 15 min at constant temperature before any measurement was performed, while at the phase transition that period was increased to at least 30 min.

4. Results

4.1. NMR spectra

Fig. 1 shows the NMR proton spectra for [C_2Im][NO_3] + $LiNO_3$ liquid and gel mixtures analysed in this work; the proton signals of the cation, printed in the inset, are labelled with numbers, 1 to 7, to facilitate the analysis. Peaks shift, in ppm, and the fitted values of Full Width at Half Maximum (FWHM), in Hz, can be found in Tables 3 and 4, respectively. From these results it can be observed that protons 1, 2 and 4 are slightly shifted up-field upon salt addition to liquid samples, especially proton 4, due to its acid character in the imidazolium ring [15,28]. However, alkyl chain protons do not show a significant shift with salt addition indicating no chemical changes of the environment. This corresponds to nanostructured solvation paradigm, according to which, salt ions are accommodated in the polar nanoregions of the liquid [29,30].

At lower field region the peak assigned to the labile N–H proton (hydrogen 5) in the imidazolium ring, at 14.48 ppm for pure IL, can be recognized, indicating a very strong proton deshielding. This result agrees with other authors that analysed imidazolium based ILs, as for example Zhu *et al.* [31] for the 1-methyl-3-imidazolium triflate and Takao and Tsubomura [32] for 1-ethyl-3-methylimidazolium tetrafluoroborate. The upper-field shifting for this labile proton of the [C_2Im][NO_3] IL associated to the deshielded N-H proton indicates that the [NO_3]$^-$ anion has a higher influence on the polar region of the imidazolium ring of the pure IL due to the formation of hydrogen bonds.

Since [C_2Im][NO_3] is considered a protic ionic liquid (PIL) due to the N-H bond, this IL could be forming H-bonds due to his donor character in the framework of Bronsted-Lowry acid/base theory, the most remarkable change with regard to salt addition corresponds specifically to proton signal of N-H, which is shifted upfield from 14.48 ppm for pure IL to 13.66 ppm for the sample with the highest salt concentration due to

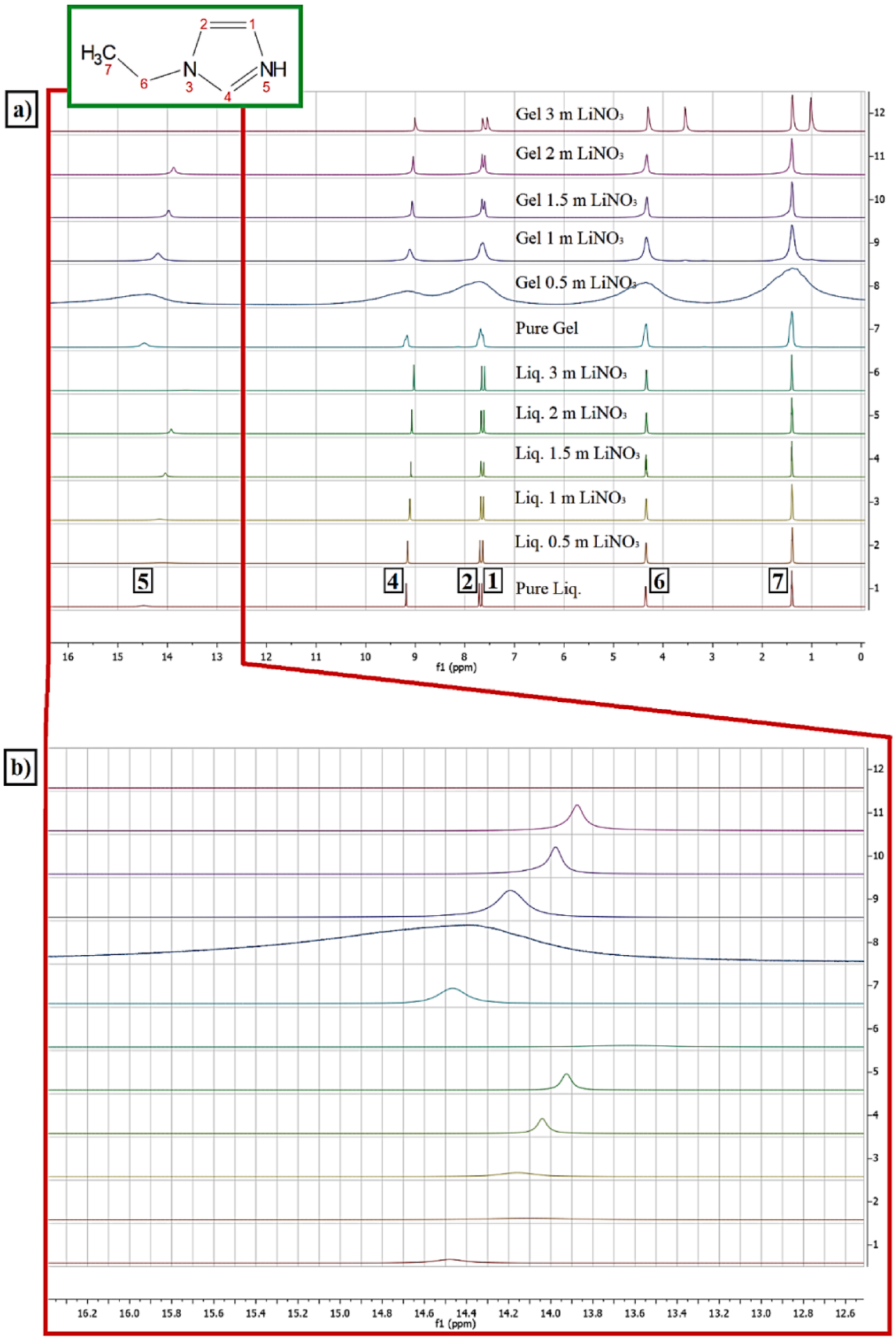

Fig. 1. A) nmr^{1}H spectra for liquid (samples 1 to 6) and gel (samples 7 to 12). Inset shows $[C_2Im]^+$, with the corresponding numbered atomic bonds. Y axis is measured with arbitrary units (A.U.). Peaks at 1.0 and 3.68 ppm in sample 12 correspond to protons in ethanol. b) The inset shows the peak corresponding to proton 5 (N-H).

Table 3
Chemical shift (in ppm) of ^{1}H spectra and ^{13}C for liquid and gel mixtures $[C_2Im][NO_3]$ + $LiNO_3$ salt of the signals presented in Figs. 1 and 2.

	Sample	7 (CH_3)	6 (CH_2)	1 (CH)	2 (CH)	4(CH)	5(NH)
	^{1}H spectra						
LIQUID	**Pure IL**	1.4 (T)	4.35 (Q)	7.66 (S)	7.71 (S)	9.19 (S)	14.48 (S)
	Mixture 0.5 m	1.4 (T)	4.35 (Q)	7.64 (S)	7.7 (S)	9.16 (S)	14.11 (S)
	Mixture 1 m	1.4 (T)	4.34 (Q)	7.63 (S)	7.68 (S)	9.11 (S)	14.16 (S)
	Mixture 1.5 m	1.4 (T)	4.34 (Q)	7.62 (S)	7.68 (S)	9.09 (S)	14.04 (S)
	Mixture 2 m	1.4 (T)	4.34 (Q)	7.61 (S)	7.67 (S)	9.07 (S)	13.93 (S)
	Mixture 3 m	1.4 (T)	4.33 (Q)	7.6 (S)	7.66 (S)	9.03 (S)	13.66(S)
GEL	**Pure IL**	1.4 (S)	4.34 (S)	7.64 (S)	7.69 (S)	9.16 (S)	14.47 (S)
	Mixture 0.5 m	1.4 (S)	4.35 (S)	7.71 (S)		9.16 (S)	14.37 (S)
	Mixture 1 m	1.4 (S)	4.34 (S)	7.64 (S)	7.69 (S)	9.11 (S)	14.19(S)
	Mixture 1.5 m	1.4 (S)	4.33 (S)	7.60 (S)	7.65 (S)	9.06 (S)	13.98 (S)
	Mixture 2 m	1.4 (S)	4.33 (S)	7.60 (S)	7.65 (S)	9.04 (S)	13.88(S)
	Mixture 3 m	1.4 (T)	4.30 (Q)	7.55 (S)	7.64 (S)	9.01 (S)	UNDEFINED
	^{13}C spectra						
LIQUID	**Pure IL**	17.54	47.19	124.36	122.9	138.13	X
	Mixture 0.5 m	17.54	47.27	124.39	122.91	137.97	X
	Mixture 1 m	17.52	47.24	124.37	122.9	137.99	X
	Mixture 1.5 m	17.52	47.38	124.49	122.96	137.96	X
	Mixture 2 m	17.49	47.38	124.47	122.94	137.88	X
	Mixture 3 m	17.47	47.33	124.39	122.88	137.76	X
GEL	**Pure IL**	17.54	47.29	124.43	122.94	138.13	X
	Mixture 0.5 m	17.54	47.23	124.32	122.76	137.84	X
	Mixture 1 m	17.54	47.36	124.47	122.96	138.01	X
	Mixture 1.5 m	17.54	47.38	124.45	122.96	137.92	X
	Mixture 2 m	17.54	47.41	124.47	122.96	137.89	X
	Mixture 3 m	17.54	47.32	124.46	122.88	137.70	X

S: singlet, T: triplet, Q: quadruplet. For carbon spectra, all detected signals were identified as a singlet.

Table 4
Fitted FWHM (in Hz) of ^{1}H and ^{13}C spectra for liquid and gel samples shown in Figs. 1 and 2. For triplet and quadruplet is presented each fitted FWHM of the peak forming multiplet.

	Liquid	7 (CH_3)	6 (CH_2)	1 (CH)	2 (CH)	4 (CH)	5 (NH)
	^{1}H spectra						
LIQUID	**Pure IL.**	5.31; 7.06; 6.67	8.97; 5.69; 6.28; 4.80	6.87	6.88	6.87	122
	Mixture 0.5 m	6.75; 9.02; 6.21	7.08; 7.25; 7.07; 6.86	7.55	7.67	7.81	356
	Mixture 1 m	6.31; 9.02; 6.31	5.98; 8.42; 6.04; 9.73	8.09	8.09	9.16	143.68
	Mixture 1.5 m	3.11; 4.75; 5.68	3.76; 2.54; 5.62; 5.45	7.53	8.26	7.56	50.02
	Mixture 2 m	8.30; 7.97; 4.87	7.65; 7.37; 6.21; 4.68	7.62	7.15	6.8	42.98
	Mixture 3 m	6.07; 4.34; 4.01	4.74; 4.20; 3.75; 3.53	7.32	7.36	7.4	325
GEL	**Pure IL.**	58.89	58.87	45.31	32.57	32.79	117.76
	Mixture 0.5 m	468	454	501		501	501
	Mixture 1 m	77.79	78.15	74.75	55.48	72.27	114.36
	Mixture 1.5 m	24.31	28.67	17.83	16.31	16.12	38.37
	Mixture 2 m	24.5	29.38	15.25	17.33	14.2	34.3
	Mixture 3 m	31.81	27.31	21.12	21.72	20.93	UNDEFINED
	^{13}C spectra						
LIQUID	**Pure IL**	7.8	19.89	7.3	6.7	10.39	X
	Mixture 0.5 m	10.39	25.24	26.86	27.53	27.45	X
	Mixture 1 m	8.4	8.5	7.4	6.8	9.9	X
	Mixture 1.5 m	11.58	10.8	10.7	10.7	15.4	X
	Mixture 3 m	5.87	6.78	11.55	7.08	7.83	X
GEL	**Pure IL.**	14.79	15.96	16.03	16.45	16.45	X
	Mixture 0.5 m	117	246.8	155.1	241.5	183.2	X
	Mixture 1 m	22.7	26.7	24.5	24.5	25.1	X
	Mixture 1.5 m	6.2	10.6	11.3	11.3	10.6	X
	Mixture 2 m	6.5	11.1	14.1	13.8	12.4	X
	Mixture 3 m	14.2	11.3	10.3	10.7	16.2	X

hydrogen bond breaks in the presence of the lithium salt (Fig. 1b).

The FWHM of this N-H peak for all samples is more than 10 times higher than the rest of the peaks of the spectra (except for IL + $LiNO_3$ at 1.5 and 2 m samples), as it can be seen in Fig. 1 and Table 4. This broadening is typically observed in substances with –OH groups due to intermolecular exchange capacity of –OH protons with protons of the protic solvents [33,34]. In our case, the broadening of this single peak can be associated to the exchangeable character of the proton of hydrogen 5, which provokes the generation and vanishing of different species, with different signals, at a too high speed to be recognized independently by the NMR, as other authors also pointed out previously [31,35].

Additionally, with the aim to compare the signal intensity of this N-H peak (hydrogen 5), the ratio between the intensities of this proton and CH_3 proton (hydrogen 7, used as reference intensity) of every ^1H spectra are presented in Table 5. It can be seen that the IL + lithium salt at 1.5 m and 2 m show the highest values of this ratio, and, interestingly, these two mixtures show the smallest FWHM values of the N-H signal (Table 4). This could be understood considering that Li^+ cations are tetrahedrically coordinated by $[NO_3]^-$ anions, as previously reported to EAN solutions with $LiNO_3$ [36]. Indeed, upon salt addition a competition between Li^+ cation and $[C_2Im]^+$ cation to coordinate with $[NO_3]^-$ anions takes place. To clarify this statement, the number of moles of $[NO_3]^-$ per Li^+ mole in the studied mixtures of IL-$LiNO_3$ was calculated and presented in Table 6. The stoichiometric concentration of anions corresponds to 2 m mixture, and an excess of $[NO_3]^-$ anions can be observed for mixtures with lower salt concentration.

At the lowest salt concentration ($LiNO_3$ 0.5 m sample) the Li^+ cation is strongly coordinated to the $[NO_3]^-$ anion from $[C_2Im][NO_3]$, and some quantity of the remaining $[NO_3]^-$ could be reacting with $[C_2Im]^+$ to form HNO_3 exchanging the N-H proton at higher velocity than NMR resolution spectra, widening this peak [31] and increasing the FWHM (Table 4). Then, a FWHM reduction is observed with the increasing salt concentration until the mixture IL + $LiNO_3$ 2 m, which corresponds to the tetrahedral coordination limit [36], the Li^+ is surrounded by four $[NO_3]^-$, narrowing the peak and the minimum of the FWHM of this peak is therefore achieved (Table 4). Conclusively, since the mixture IL + $LiNO_3$ 3 m exceeds the stoichiometric concentration, the tetrahedral coordination is no longer exclusive, and ordered phases are no longer possible, disordered configurations are being registered again with the consequent increase in the width of the peak.

Regarding the effect of confinement, it is important to indicate that no reference capillary was used for gel samples due to their quasi-solid state, CH_3 signal at 1.4 ppm, obtained in liquid state, was used as a reference. As it can be seen in Fig. 1a) the peaks appear at the same positions as those in liquid state. However, a significant broadening occurs in all recorded signals, but they are defined enough to consider it as an indicative of a liquid-like behaviour, as Le Bideau and collaborators suggested [2,14]. This broadening for all samples, except for 0.5 m, indicates a slight slowing down on molecular dynamics, and possibly a difference in molecular environment between IL molecules that are in the pore centre and those near the polymer backbone [37]. For IL + $LiNO_3$ 3 m sample, two additional peaks are observed, probably corresponding to ethanol that was not possible to evaporate despite the purification process applied after gelation, as it is further corroborated by NMR ^{13}C (Fig. 2) spectrum.

The most interesting and unexpected signal corresponds to ionogel 0.5 m $LiNO_3$ mixture, whose ^1H and ^{13}C spectra are the widest (Figs. 1 and 2). This behaviour is very close to a solid behaviour, although the peaks are too defined to be those of a solid. This broadening is wide enough to hide some details, such as the signals of peaks 1 and 2, which have been overlapped and it is not possible to distinguish between the two proton signals. So, in this case, molecular dynamics of $[C_2Im]^+$ is slowing down to a greater extent than the other samples.

Table 5
Relative intensity of NH signal versus CH_3 signal proton spectra obtained from Fig. 1.

	Sample	$I_{N\text{-}H}/I_{CH3}$
LIQUID	**Pure IL**	0.028
	Mixture 0.5 m	0.013
	Mixture 1 m	0.034
	Mixture 1.5 m	0.112
	Mixture 2 m	0.141
	Mixture 3 m	0.012
GEL	**Pure IL**	0.119
	Mixture 0.5 m	0.295
	Mixture 1 m	0.208
	Mixture 1.5 m	0.205
	Mixture 2 m	0.202
	Mixture 3 m	UNDEFINED

Table 6
Number of $[NO_3]^-$ mol per Li^+ mol in IL + Li salt samples.

$LiNO_3$ Concentration	$[NO_3]^-$ /mol (for each added Li^+ mol)
0.5 m	13.4
1 m	7.3
1.5 m	5.2
2 m	4.0
3 m	2.1

4.2. Thermal behaviour

4.2.1. DSC results

Curves corresponding to DSC cooling and heating ramps at 5 °C·min^{-1} in nitrogen atmosphere of $[C_2Im][NO_3]$ pure liquid (a) and pure ionogel (b) are shown in Fig. 3. Pure IL shows, upon heating, an endothermic peak with onset at 35 °C and maximum at 40 °C related with the melting process of the IL. Upon cooling, an exothermic peak with onset temperature at −15 °C, associated with the freezing of the sample, is observed. Similarly to other ILs, an important supercooling effect has been observed [38,39]. This IL presents a strong tendency to form crystals in these conditions, and no evidence of any amorphous phase has been observed in the liquid state within the studied temperature range. The scarce information of the thermal behaviour of this IL includes the work of Ohno and Yoshizawa [40], who found the melting of pure $[C_2Im][NO_3]$ at 31 °C with no evidence of glass transition in in the temperature range −150 to 200 °C, in good concordance with our results. Additionally, Abe *et al.* [41] found a crystallization at −3.8 °C obtained by visual cloud-point determination with cooling rate of 1.5 °C min^{-1}. The apparent discrepancy with our results can be explained according to the different methodology used and, in any case, is consistent with the different cooling rates used by these authors and us.

One of the most remarkable effects reported in the limited literature regarding to pure ILs confinement in the silica network is that the first-order transitions are often suppressed, due to small available space for the IL crystallization after gelation [2,42]. In our case, DSC curves of ionogels (Fig. 3b) showed similar peaks to those of the liquid samples [2], although melting and freezing peaks of ionogel samples are significantly shifted to lower temperatures ($\Delta T_{melting} = -35$ °C and $\Delta T_{freezing} = -34$ °C) and peak signals are widened relative to those of the bulk liquid samples. It is well known that the melting points of pure materials are characterized by simple and sharp peak, while impure or polymeric samples display more broader peaks. Impurities and some possible rests of gelation have been removed firstly with a high vacuum process after the gelation and additionally, before the thermal ramps with a previous isothermal step at high temperature, as it was pointed out in material and methods section. Therefore, the widening effect must be associated to confinement, as it is also commented in the literature [2]. Additionally, Kanakubo *et al.* [19] indicate that the peak widening and the

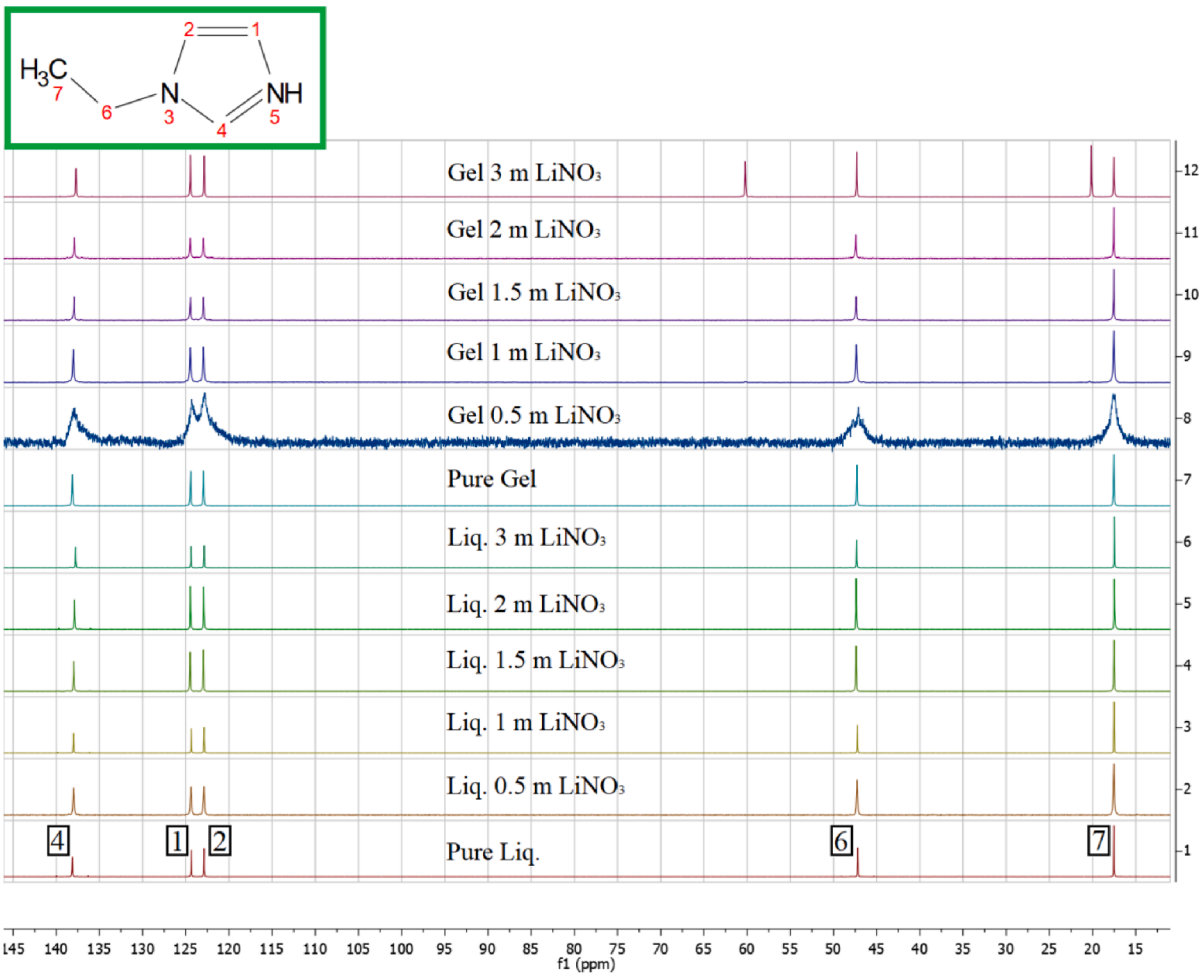

Fig. 2. NMR ^{13}C spectra for liquid (samples 1 to 6) and gel (samples 7 to 12). Inset shows $[C_2Im]^+$, with the corresponding numbered atomic bonds. Y axis is measured with arbitrary units (A.U.). Not tagged peaks in sample 12 correspond to ethanol peaks.

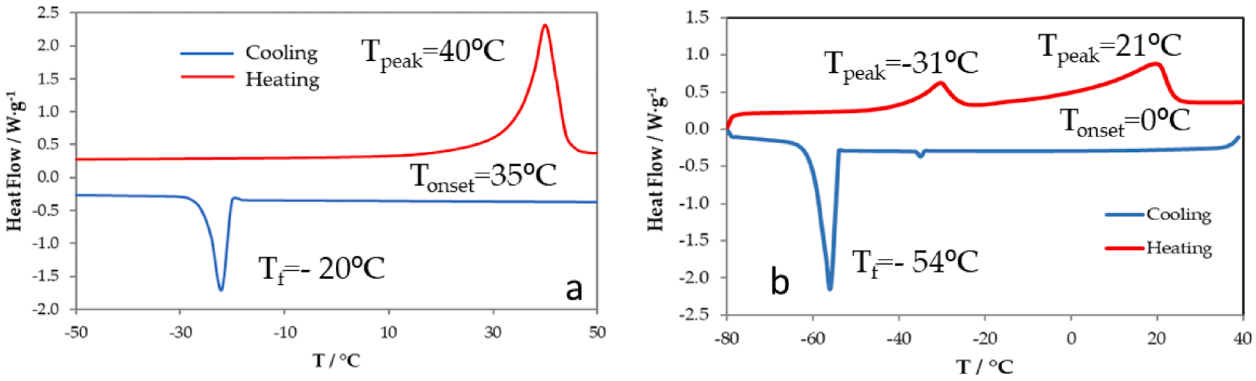

Fig. 3. DSC curves (exo down) in heating and cooling ramps of pure $[C_2Im][NO_3]$ in liquid form (a) and in gel form (b).

temperature depression of melting after nanoconfinement are both proportional to the inverse of the pore diameter. These authors also highlight that the melting temperature depression increases with the hydrophilicity of the IL, in good agreement with our observations for this highly hydrophilic IL.

Gel samples also show an additional small peak around −30 °C. Other important effect of the confinement due to the high-density charge inside the pore, also underlined in literature [15,19,43], is the formation of different metastable solids inside the matrix, which present different melting temperatures.

Fig. 4 shows the comparison between DSC curves corresponding to heating and cooling ramps for liquid samples of $[C_2Im][NO_3]$ + $LiNO_3$ mixtures at the different concentrations. Although similar behaviour of pure IL can be observed for the lowest concentration, the addition of salt tends to reduce the supercooling effect, previously observed in pure IL. Moreover, the concentration of salt in the mixture has two important effects on the thermal behaviour. Firstly, a clear decrease of the melting temperature as expected [24], together with a reduction of the intensity and a broadening of the peak are observed. These remarks are indicative of a reduction of the sample crystallinity with the increase of salt

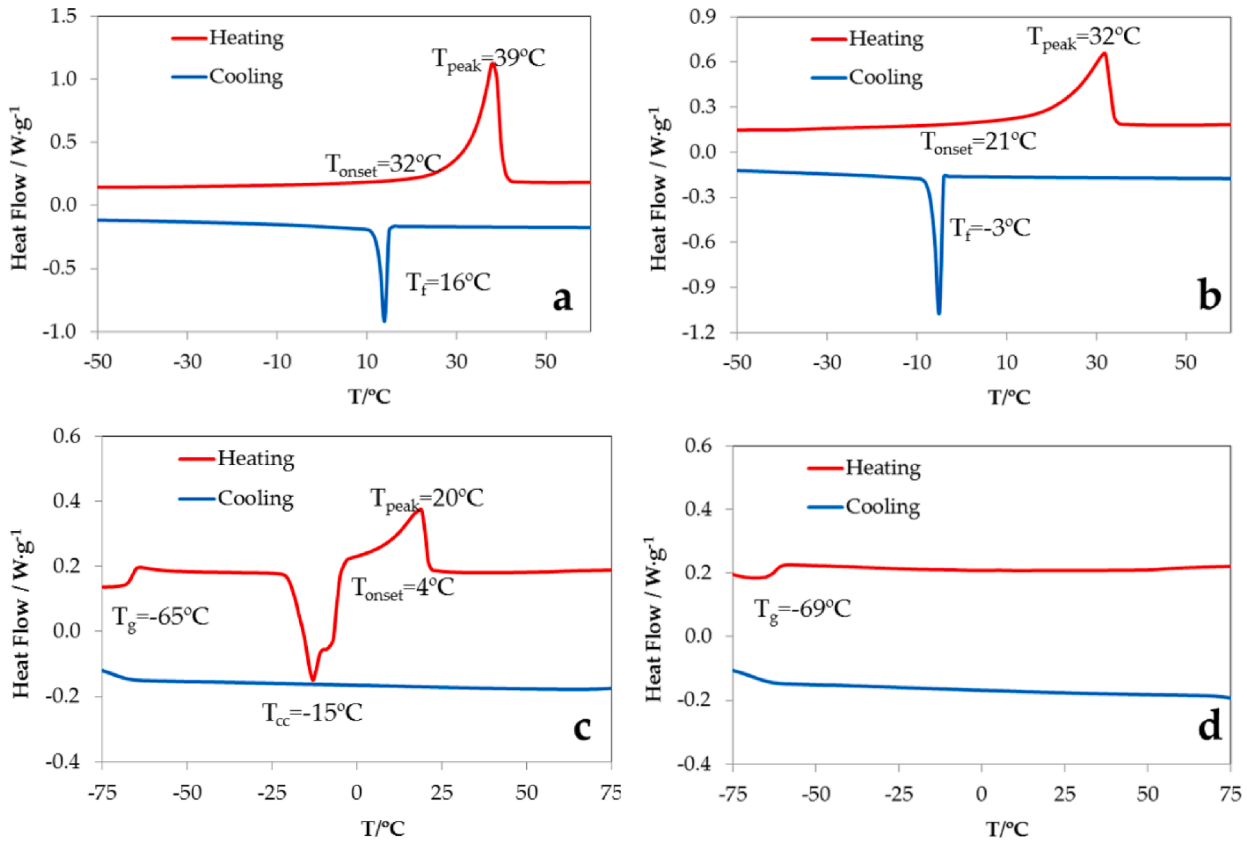

Fig. 4. DSC curves (heating and cooling ramp) of liquid metal salt solutions, (a) 0.5 m, (b) 1 m, (c) 2 m and (d) 3 m (exo down).

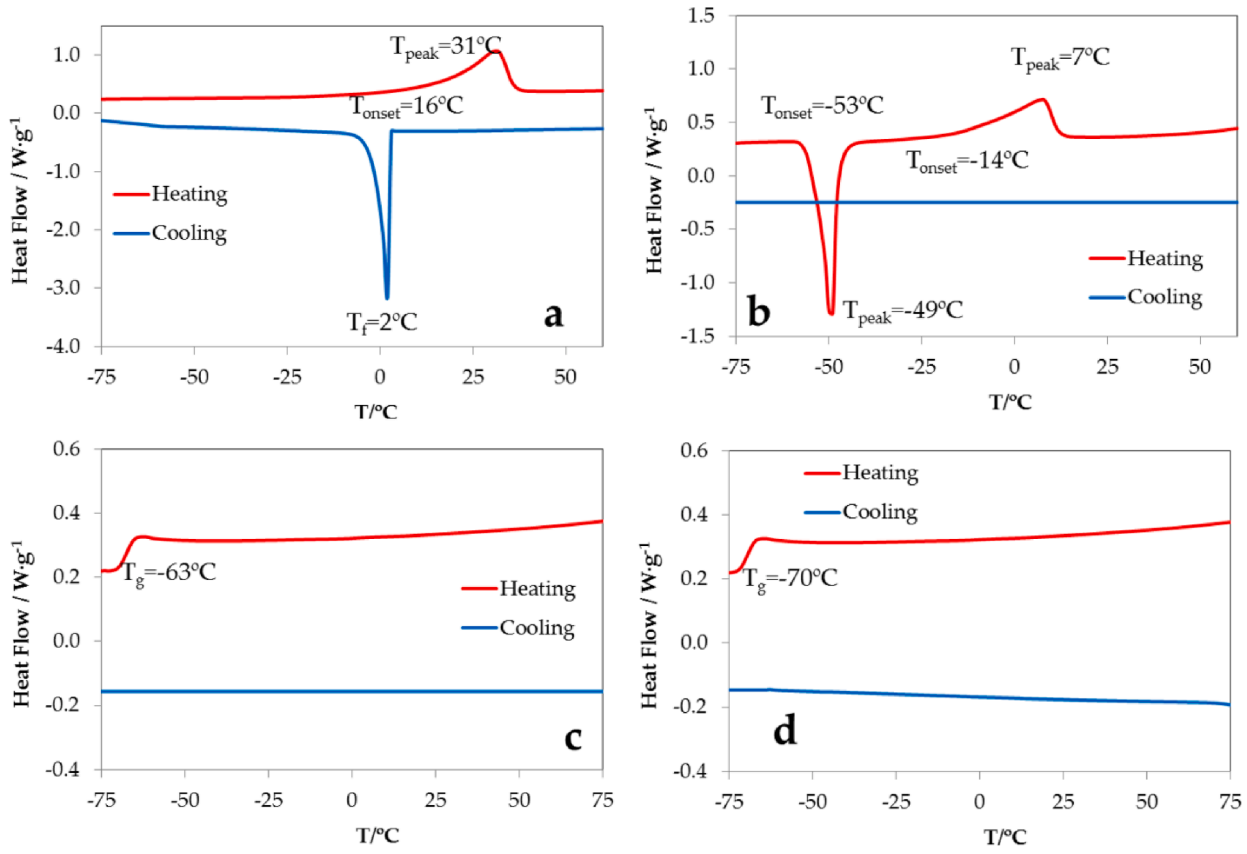

Fig. 5. DSC curves (heating and cooling ramp) metal salt solutions in gel form, (a) 0.5 m, (b) 1 m, (c) 2 m and (d) 3 m (exo down).

concentration, which is especially visible for the two highest concentrations, 2 and 3 m (Fig. 4c and d, respectively), where no crystallization is observed upon cooling, and a glass transition at lower temperatures is clearly visible for both mixtures. Particularly, IL + salt 2 m sample achieves a cold-crystallization (exothermic peak) upon heating with the consequent melting peak. Nevertheless, in case of 3 m mixture no evidence of crystalline behaviour can be observed, presenting uniquely a glass transition at −69 °C, that is representative of a completely amorphous behaviour, with the subsequent liquid range extension. This fact would imply the important role that this mixture could have on refrigeration and storage at very low temperatures and other applications requiring very low (or even very high) temperatures. These results agree with previous observations (of NMR in this paper and computer simulation in previous works of some of us [29,30,36]) that the addition of lithium salt provokes the formation of nanocrystals in the polar region of the IL, then these ordered structures melt at temperatures that decrease with the salt concentration until the tetrahedral coordination concentration (2 m) is achieved. For the highest salt concentration, the ordered phases are frustrated, provoking the vanishing of the DSC peaks. It is especially interesting the thermal behaviour of mixture of 2 m, that corresponds to 4 mol of nitrate anion for every lithium cation (see Table 6); the DSC signal does not show any transition upon cooling, which indicates a completely amorphous behaviour of the systems, with a low ordering degree of the ions in the polar nanoregion. In fact, a glass transition is the first transition observed, when starting the next heating ramp. However, this critical concentration leads to a tendency to crystallize, and new crystals are formed upon heating, appearing the exothermic peak of cold crystallization at −15 °C with the subsequent melting process.

DSC curves corresponding to heating and cooling ramps of ionogel samples of $[C_2Im][NO_3]$ + $LiNO_3$ mixtures at different concentrations are shown in Fig. 5. Similarly to ionogel of pure IL, the confinement of mixtures in the silica network shows important similarities to the corresponding liquid mixture, that is evidence of liquid state inside the pores as it was noted in NMR results, although this confinement emphasizes the reduction of supercooling effect and loss of crystallinity with the salt addition concentration. Consequently, only the DSC curves of the lowest concentration of Li salt present freezing and melting peaks in cooling and heating ramps respectively, which implies the existence of ordered structures within the matrix, although this order is broken earlier than in case of liquid sample, as its melting temperature decreases from 32 °C to 16 °C. The $[C_2Im][NO_3]$ + $LiNO_3$ 1 m mixture (Fig. 5b) shows a cold crystallization peak at −53 °C followed by a broader melting peak upon heating, which is an indicative of crystallization failure upon cooling, although this clear ordering trend is maintained in heating ramp. The confinement of the most concentrated mixtures (2 and 3 m) frustrates completely the crystallization (only glass transition can be observed in DSC curves). Ordered phases are not possible inside the cavities of the silica scaffold because of high lithium salt concentrations.

4.2.2. *Thermal stability*

Thermogravimetric (TG) and Differential Thermal Analysis (DTA) curves of pure $[C_2Im][NO_3]$ under nitrogen atmosphere and with a heating rate of 10 °C min^{-1} are shown in Fig. 6. DTA and TG signals exhibit a unique loss step (endothermic peak) at the same temperature interval indicating that vaporization is the main mechanism of degradation of the IL. A loss of 4 % of the initial mass takes place up to 110 °C, corresponding to the release of water and some synthesis volatile substances. The highest mass loss step (85 % loss) appears between 160 and 226 °C with the maximum rate at 207 °C. Up to our knowledge no data of thermal stability of this IL can be found in literature, although these results are consistent with the idea that protic ILs frequently present lower thermal stabilities than aprotic ILs, due to the proton transfer from the salt form to precursor acid/base pairs [15]. Furthermore, as it is well known, the thermal stability depends strongly on the anion of the IL; being nitrate anion associated with low thermal stability [44]. $[C_2Im][NO_3]$ presents similar short-term stability temperatures, around 200 °C, than other nitrate based ILs, as EAN [24]. It is important to note that the long-term thermal stability of ILs is much lower than the decomposition temperatures obtained by step-tangent TG analysis, and, although it is not the aim of this work to analyse it deeply, a good way to estimate it [44] is using the suggestion of Wooster *et al.* [45] and Baranyai *et al.* [46]. Following this criterion, a value of 130 °C was obtained for this pure IL.

Fig. 7a shows the TG and DTA curves of $[C_2Im][NO_3]$ + $LiNO_3$ saturated mixture (3 m) in liquid form obtained under nitrogen atmosphere at 10 °C min^{-1}, where two main steps in TG curve coincident with two endothermic peaks in DTA thermogram at 223 and 338 °C can be observed. The mass loss corresponding to the first step is almost 60 % of the initial weight of the sample and it is slightly shifted to higher temperatures comparing with pure IL, as it is shown in Fig. 7b, *i. e.*,

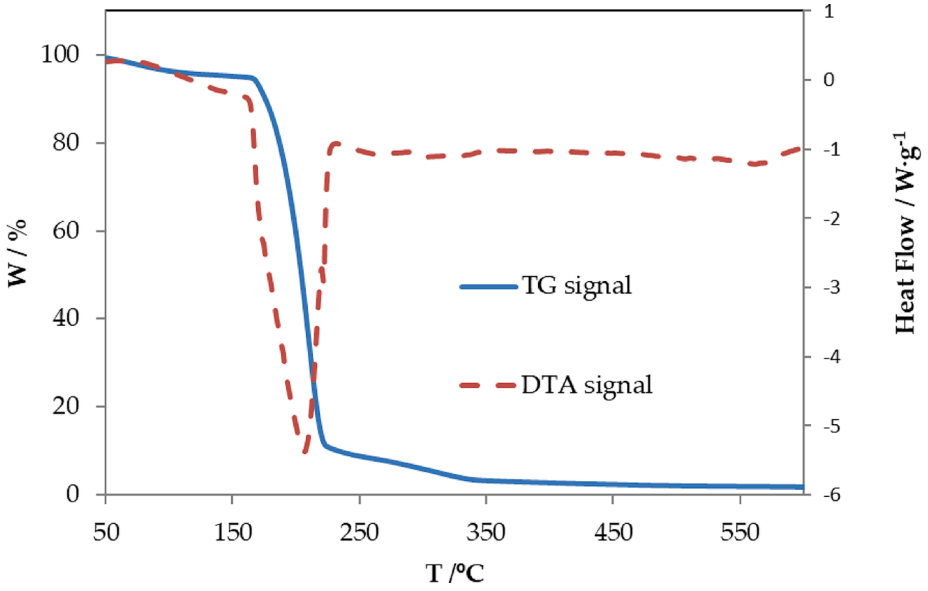

Fig. 6. TG (blue line) and DTA (red line) curves (endo down) of pure $[C_2Im][NO_3]$ under nitrogen atmosphere at 10 °C min^{-1}. (For interpretation of the references to colour in this figure legend, the reader is referred to the web version of this article.)

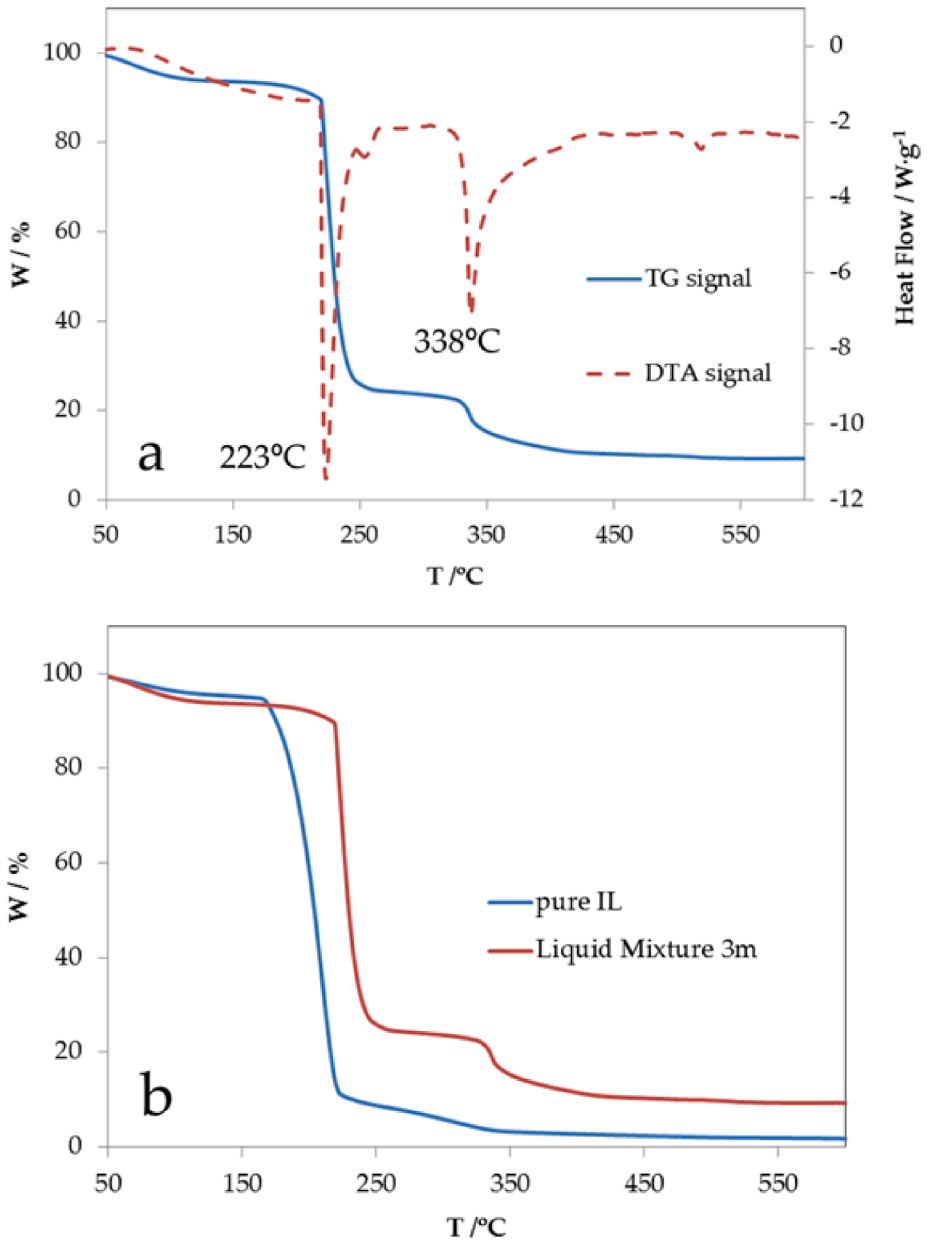

Fig. 7. TG and DTA curves (endo down) of saturated mixture of $[C_2Im][NO_3]$ + $LiNO_3$ salt in liquid form under nitrogen atmosphere at 10 °C min^{-1} (a), comparison between TG curves of pure IL and saturated mixture (b).

thermal stability of the mixture is slightly higher than that of the pure IL. The lithium salt of the mixture and the secondary products of degradation are the cause of the second peak in the TG and DTA curves of the mixture.

Fig. 8a and b show the TG and DTA curves of pure ionogel, and the comparison of TG traces corresponding to the liquid and gel forms, respectively. As it can be observed, the gelation process has no significant effects on the thermal stability.

4.3. Ionic conductivity

Fig. 9 shows the conductivity data obtained from heating and cooling ramps for pure $[C_2Im][NO_3]$, liquid (a) and gel (b) states, respectively. Hysteresis is clearly visible in both, liquid and gel, characterized, upon heating, by an almost vanishing ionic conductivity until 303 K, which is concordant with the melting point observed from DSC analysis of liquid and gel samples. Nevertheless, higher values of ionic conductivity can be observed in cooling ramps at each temperature, according to the supercooling effect, also observed in thermal behaviour of these samples. For this reason, ionic conductivity of all liquid and gel samples (pure and lithium salt doped) were measured upon cooling. Results are summarized in Fig. 10. As expected, this property increases with temperature for all studied liquid and ionogel samples. For the same concentration of lithium salt, the lowest ionic conductivity corresponds to the ionogel sample, except for the highest salt concentration, in which practically no difference has been observed between liquid and gel samples, probably, due to the small amount of ethanol remaining in the sample despite the purification step, as it was remarked in the NMR section. The most important observation with regards to ionic conductivity is that the trend observed with salt addition is different for liquid and gel samples. While ionic conductivity decreases in liquid samples with salt addition (Fig. 11a) as it can be expected and is widely reported in literature due to higher viscosity because of strongly interacting mixtures [23,29,47], for ionogels, this property reaches a maximum at

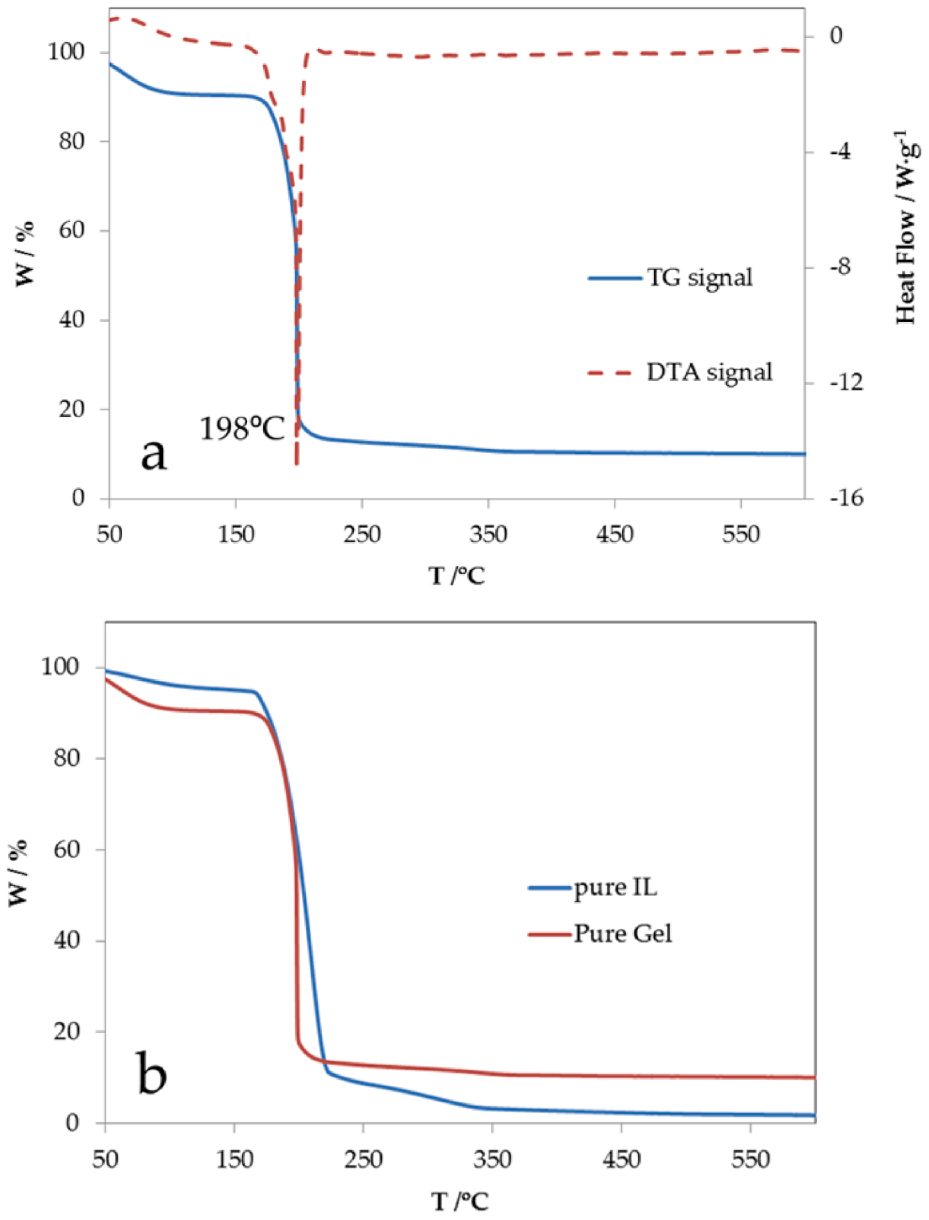

Fig. 8. TG and DTA curves (endo down) of pure $[C_2Im][NO_3]$ in gel form under nitrogen atmosphere at 10 °C min^{-1} (a), comparison between TG curves of pure IL in liquid and gel forms (b).

the lowest salt concentration studied (0.5 mol/kg_{IL}) followed by the expected decrease with salt addition (Fig. 11b). For example, at 323 K and 0.5 m salt concentration the conductivity of this ionogel is 13.26 mS·cm^{-1}, which represents a 12 % higher than the ionogel of pure IL (12.16 mS·cm^{-1}) at the same temperature. The increase in this property after gelation could be, initially, related with the presence of water in the sample, but NMR characterization does not show significant water quantities (or other cosolvents) present in the analysed sample, as it was reported previously. We have also observed this behaviour in ionogels of ethylammonium nitrate and lithium nitrate mixtures [25]. This effect can be, then, associated to the confinement of liquid in the silica host network. While clusters of ions can be formed in liquid mixtures with zero net charge, implying that diffusive species do not contribute to conductivity, the interactions with silica scaffold could decrease the electrostatic force of attraction between ions. Thus, the tendency to form ion clusters or aggregates diminishes, resulting in an increase in the amount of ion carriers and subsequently enhancing ionic conductivity. It is important to highlight again the width of the peaks of NMR of the ionogel of the mixture IL + salt 0.5 m, associated to the slowing down dynamics of the cation $[C_2Im]^+$; then, this ionic conductivity increase seems to be related with the enhancement in mobility of free lithium ions or other lithium complexes through the conductive paths inside the ionogel. Interestingly, ĎAngelo and Panzer [48] found an increase in lithium transference number after the confinement of lithium salt/pyrrolidinium IL solution 1 M in a cross-linked polymer gel attributed to favourable interactions between the polymer network and ionic species that cause an increase in ion separation that means a higher ion mobility. Although studies on ionic conductivity after confinement can be found in literature [1,3,14,19,21,49–53], the analysis of the dependence of the combined effect of salt addition and confinement against salt concentration is scarce and results seem indicate that this concentration must have an important role in the performance of quasi-solid electrolytes. To consolidate these results, further studies with different ILs + salt mixtures nanoconfined in scaffolds of different natures are necessary. It is important to note that large values of the Li^+ transference number are desirable to avoid the accumulation of other mobile ions in

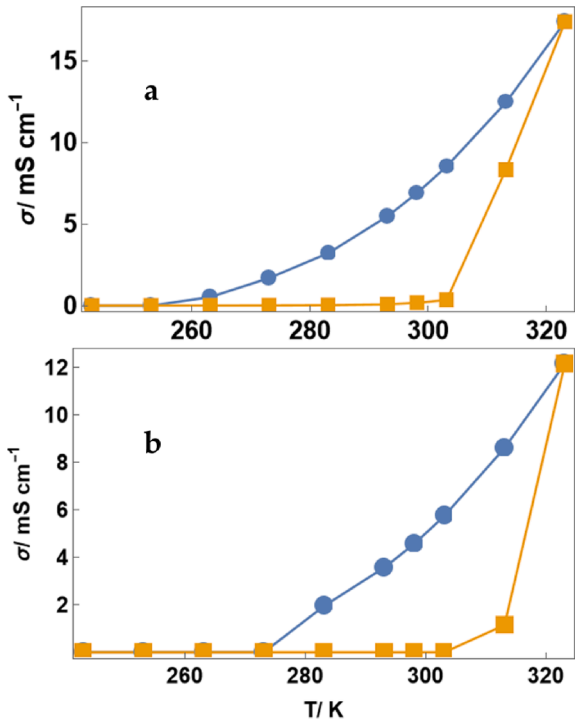

Fig. 9. Conductivity vs Temperature for heating ramp (orange squares) and cooling ramp (blue dots) for a) $[C_2Im][NO_3]$ pure liquid, and b) $[C_2Im][NO_3]$ pure gel. The lines act as guides to the eye. (For interpretation of the references to colour in this figure legend, the reader is referred to the web version of this article.)

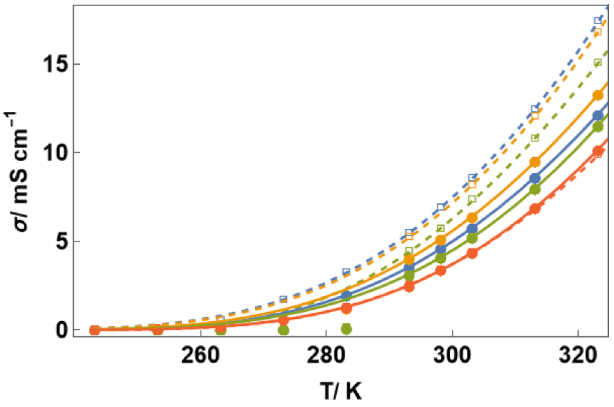

Fig. 10. Comparison of the electrical conductivity of $[C_2Im][NO_3]$ + $LiNO_3$ mixtures versus temperature of liquid (empty squares) and gel (filled dots): pure $[C_2Im][NO_3]$ (blue), $[C_2Im][NO_3]$ + $LiNO_3$ at 0.5 m (orange), $[C_2Im][NO_3]$ + $LiNO_3$ at 1 m (green) and $[C_2Im][NO_3]$ + $LiNO_3$ at 3 m (red). Lines correspond to the fitting to the VFT equation. (For interpretation of the references to colour in this figure legend, the reader is referred to the web version of this article.)

the system (*i.e.*, $[C_2Im]^+$ and $[NO_3]^-$) at the surface of the electrodes, increasing the thickness of the passivation films and preventing the lithium ion from reaching the active surface of the electrode [48].

Experimental data of ionic conductivity upon cooling can be fitted against temperature by Vogel-Fulcher-Tammann equation (VFT) (eq. (1) in intervals where no phase transition is observed [54–56].

$$\sigma = \sigma_\infty exp\left[-\frac{E_a}{k_b(T-T_g)}\right] \quad (1)$$

Table 7 shows the obtained parameters from VFT fitting for liquid and gel samples, where a decrease of σ_∞ with salt concentration on liquid samples is visible. This fact is in contrast with the behaviour of gel samples, where an increase of this parameter with salt addition is observed. The activation energy (E_a) values seem to remain at a constant value with salt addition for both liquid and gel samples. The ideal glass transition temperature (T_g) ranges from 174 to 210 K in the studied samples, that is in good agreement with thermal analysis results.

5. Conclusions

This work analyses the effect of the addition of lithium salt and the subsequent confinement on a silica scaffold of the protic IL, ethylimidazolium nitrate, in terms of the structural changes measured by NMR spectroscopy, the thermal behaviour by DSC and TGA and the ionic conductivity. The main results are the following:

NMR spectra provided evidence of nanostructural segregation of the IL and a further solvation of salts in the highly ionic environment, and also a broadening of the peaks as a consequence of the confinement indicating a solid-like behaviour but preserving the liquid properties inside the silica scaffold.

The addition of salt does not inhibit melting peak (upon heating) and crystallization peak (upon cooling) for the two lowest concentrations, but the melting temperature decreases with the salt addition. The highest concentration of salt inhibits the crystalline phase, and a single glass transition is visible in heating ramp. In contrast to other PILs, the nanoconfinement of the pure IL does not inhibit neither the crystallization nor the melting observed in liquid samples. Only shifts towards lower temperatures and a widening of the corresponding peaks were observed, indicating a liquid behaviour inside the silica matrix, with concordance of NMR results. The superposition of the salt addition and the confinement tend to increase the disorder in the polar nanoregions, but to a lesser extent than other PILs, since the crystallization is only frustrated for the highest salt concentration (3 m) in liquid state and for the two highest salt concentrations in ionogel state.

The ionic conductivity of the liquid samples follows the expected behaviour, increasing with temperature and decreasing with salt concentration. Interestingly, the confinement does not significantly reduce the ionic conductivity with regards to the liquid sample, and in all the cases, values higher than the stablished limit of this parameter to be used in electrochemical devices (1 $mS{\cdot}cm^{-1}$) were obtained. Nevertheless, the most important finding of this work was an unexpected behaviour with the salt concentration in ionogel samples: this property shows a maximum in confined sample of 0.5 m IL + $LiNO_3$ mixture, approximately 12 % higher than the pure ionogel. This effect is associated to an increase in mobile charged species within an ordered background defined in the polar nanoregions of the ionogel. Although further studies must be performed to fully understand the mechanism behind these observations.

CRediT authorship contribution statement

P. Vallet: Conceptualization, Data curation, Writing – original draft. **J.J. Parajó:** Data curation, Formal analysis, Methodology, Validation, Writing – original draft. **A. Santiago-Alonso:** Data curation, Methodology, Software. **M. Villanueva:** Data curation, Formal analysis, Funding acquisition, Methodology. **Ó. Cabeza:** Conceptualization, Formal analysis, Methodology, Writing – review & editing. **L.M. Varela:** Conceptualization, Formal analysis, Funding acquisition, Supervision, Validation, Writing – review & editing. **J. Salgado:** Conceptualization, Formal analysis, Funding acquisition, Investigation, Methodology, Resources, Supervision, Validation, Visualization, Writing – original draft, Writing – review & editing.

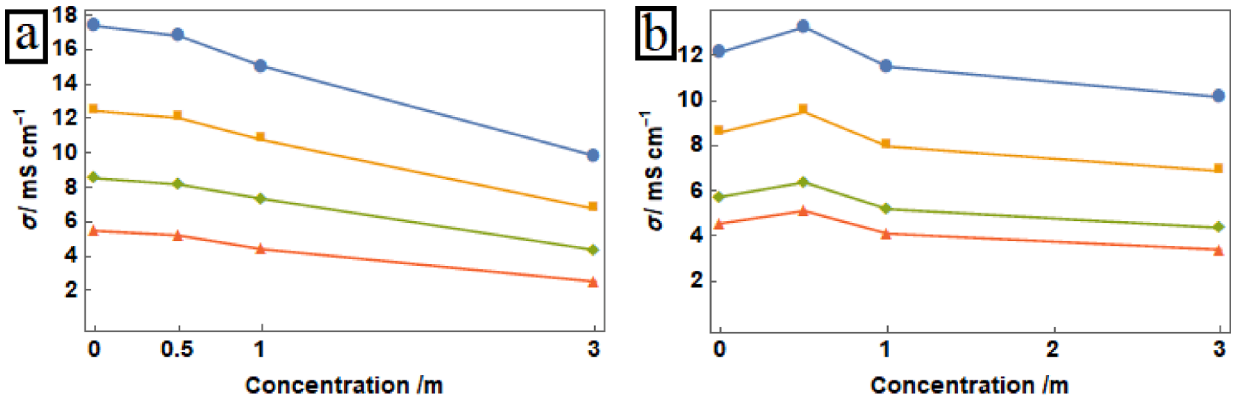

Fig. 11. Comparison of the electrical conductivity versus the concentration (mol kg^{-1}) of Li^+ salt in liquid mixtures a), and in gel mixtures b) (0 concentration refers to pure [C_2Im][NO_3]) at different temperatures: 323 K (blue dots), 313 K (orange squares), 303 K (green diamonds) and 293 K (red triangles). The lines act as a guide for a better visualization.

Table 7
Physical magnitudes and corresponding standard deviations obtained from the fitting of experimental conductivity on cooling ramp of the pure and doped liquid and gel samples to VFT equation (eq. (1).

Sample	σ_∞/mS cm^{-1}	E_a/ eV (x10^{-3})	T_g/K
Pure Liq.	1730 ± 190	59 ± 3	174 ± 3
$LiNO_3$ 0.5 m Liq.	1770 ± 100	59.9 ± 1.4	174 ± 2
$LiNO_3$ 1 m Liq.	500 ± 200	34 ± 9	210 ± 13
$LiNO_3$ 3 m Liq.	740 ± 50	46.8 ± 1.4	192 ± 2
Pure Gel	810 ± 100	47 ± 3	191 ± 3
$LiNO_3$ 0.5 m Gel	1000 ± 200	51 ± 5	185 ± 6
$LiNO_3$ 1 m Gel	1500 ± 300	60 ± 4	180 ± 5
$LiNO_3$ 3 m Gel	1300 ± 200	55 ± 3	189 ± 4

Declaration of competing interest

The authors declare the following financial interests/personal relationships which may be considered as potential competing interests: L. M. Varela, J. Salgado, M. Villanueva reports financial support was provided by Government of Galicia Department of Culture Education and Universities. Pablo Vallet reports financial support was provided by FPI program. Spanish Government. Juan Jose Parajo reports was provided by Axencia Galega de Innovación. Antia Santiago-Alonso reports financial support was provided by Axencia Galega de Innovación. L.M. Varela, J. Salgado, M. Villanueva reports financial support was provided by Spanish Scientific Research Council. If there are other authors, they declare that they have no known competing financial interests or personal relationships that could have appeared to influence the work reported in this paper.

Data availability

Data will be made available on request.

Acknowledgements

Authors acknowledge M. Gómez and M. Martín-Pastor (RIAIDT-USC) for their technical support in DSC and NMR measurements, respectively. This work was founded by Spanish Ministry of Economy and Competitiveness and FEDER Program through the project MAT2017-89239-C2. Vallet, J. J. Parajó and A. Santiago-Alonso thank funding support of FPI Program from Spanish Ministry of Science, Education and Universities, I2C postdoctoral and predoctoral Programs of Xunta de Galicia, respectively.

References

[1] L. Negre, B. Daffos, V. Turq, P.L. Taberna, P. Simon, Ionogel-based solid-state supercapacitor operating over a wide range of temperature, Electrochim. Acta 206 (2016) 490–495, https://doi.org/10.1016/j.electacta.2016.02.013.
[2] J. Le Bideau, L. Viau, A. Vioux, Ionogels, ionic liquid based hybrid materials, Chem. Soc. Rev. 40 (2011) 907–925, https://doi.org/10.1039/c0cs00059k.
[3] I.H. Sajid, M.F.M. Sabri, S.M. Said, M.F.M. Salleh, N.N.N. Ghazali, R. Saidur, B. Subramaniam, S.W. Hasan, H.A. Jaffery, Crosslinked thermoelectric hydro-ionogels: A new class of highly conductive thermoelectric materials, Energy Convers. Manag 198 (2019), https://doi.org/10.1016/j.enconman.2019.111813.
[4] S. Rana, R.C. Thakur, H.S. Dosanjh, Ionic liquids as battery electrolytes for lithium ion batteries: Recent advances and future prospects, Solid State Ion. 400 (2023), https://doi.org/10.1016/j.ssi.2023.116340.
[5] O. Cabeza, J.H. Fernández, F.M. Gaciño, J. Salgado, M. Villanueva, J.A. Nóvoa López, H. Michinel, E.L. Lago, L. Segade, T. Méndez-Morales, L.M. Varela, A.M.A. M. Rubio, F. Tomás-Alonso, J.H. Fernández, A.P. de los Ríos, F.J.H. Fernández, J. Hernández-Fernández, A. Pérez de los ríos, Hernández Fernández, F.J.Green aspects of ionic liquids, in: A. Pérez de los Ríos, F.J. Hérnández Fernández (Eds.), Ionic Liquids in Separation Technology, Elsevier, Amsterdam, 2014, pp. 82–93, https://doi.org/10.1016/B978-0-444-63257-9.00001-8.
[6] J. Salgado, T. Regueira, L. Lugo, J. Vijande, J. Fernández, J. García, Density and viscosity of three (2,2,2-trifluoroethanol+1-butyl-3-methylimidazolium) ionic liquid binary systems, J. Chem. Thermodyn. 70 (2014) 101–110, https://doi.org/10.1016/j.jct.2013.10.027.
[7] D. Hekmat, D. Hebel, S. Joswig, M. Schmidt, D. Weuster-Botz, Advanced protein crystallization using water-soluble ionic liquids as crystallization additives, Biotechnol. Lett. 29 (2007) 1703–1711, https://doi.org/10.1007/s10529-007-9456-9.
[8] M. Petkovic, J. Ferguson, A. Bohn, J. Trindade, I. Martins, M.B. Carvalho, M. C. Leitao, C. Rodrigues, H. Garcia, R. Ferreira, K.R. Seddon, L.P.N. Rebelo, C. Silva Pereira, Exploring fungal activity in presence of ILs, Green Chem. 11 (2009) 889–894.
[9] J.B. Goodenough, Evolution of strategies for modern rechargeable batteries, Acc. Chem. Res. 46 (2013) 1053–1061, https://doi.org/10.1021/ar2002705.
[10] M. Cvjetko Bubalo, S. Vidović, I. Radojčić Redovniković, S. Jokić, Green solvents for green technologies, J. Chem. Technol. Biotechnol. 90 (2015) 1631–1639, https://doi.org/10.1002/jctb.4668.
[11] P. Hapiot, C. Lagrost, Electrochemical reactivity in room-temperature ionic liquids, Chem. Rev. 108 (2008) 2238–2264, https://doi.org/10.1021/cr0680686.
[12] M. Galiński, A. Lewandowski, I. Stepniak, Ionic liquids as electrolytes, Electrochim. Acta 51 (2006) 5567–5580, https://doi.org/10.1016/j.electacta.2006.03.016.
[13] L.M. Varela, J. Carrete, M. García, L.J. Gallego, M. Turmine, E. Rilo, O. Cabeza, Pseudolattice theory of charge transport in ionic solutions: Corresponding states law for the electric conductivity, Fluid Phase Equilib. 298 (2010) 280–286, https://doi.org/10.1016/j.fluid.2010.08.013.
[14] T.K.N. Tran, A. Guyomard-Lack, C. Cerclier, B. Humbert, G. Colomines, J.F. Pilard, R. Deterre, J. Le Bideau, E. Leroy, Natural rubber-based ionogels, J. Renew. Mater. 6 (2018) 251–258, https://doi.org/10.7569/JRM.2017.634174.
[15] S. Zhang, J. Zhang, Y. Zhang, Y. Deng, Nanoconfined ionic liquids, Chem. Rev. 117 (2017) 6755–6833, https://doi.org/10.1021/acs.chemrev.6b00509.
[16] K.L. Stefanopoulos, G.E. Romanos, O.C. Vangeli, K. Mergia, N.K. Kanellopoulos, A. Koutsioubas, D. Lairez, Investigation of confined ionic liquid in nanostructured materials by a combination of SANS, contrast-matching SANS, and nitrogen adsorption, Langmuir 27 (2011) 7980–7985, https://doi.org/10.1021/la201261r.
[17] C. Calahoo, L. Wondraczek, Ionic glasses: Structure, properties and classification, J. Non-Cryst. Solids: X 8 (2020), https://doi.org/10.1016/j.nocx.2020.100054.
[18] A. Guyomard-Lack, P.E. Delannoy, N. Dupré, C.V. Cerclier, B. Humbert, J. Le Bideau, Destructuring ionic liquids in ionogels: Enhanced fragility for solid devices, PCCP 16 (2014) 23639–23645, https://doi.org/10.1039/c4cp03187c.

[19] M. Kanakubo, Y. Hiejima, K. Minami, T. Aizawa, H. Nanjo, Melting point depression of ionic liquids confined in nanospaces, Chem. Commun. (2006) 1828–1830, https://doi.org/10.1039/b600074f.
[20] S. Chen, G. Wu, M. Sha, S. Huang, Transition of ionic liquid [bmim][PF6] from liquid to high-melting-point crystal when confined in multiwalled carbon nanotubes, J. Am. Chem. Soc. 129 (2007) 2416–2417, https://doi.org/10.1021/ja067972c.
[21] S.A.M. Noor, P.M. Bayley, M. Forsyth, D.R. MacFarlane, Ionogels based on ionic liquids as potential highly conductive solid state electrolytes, Electrochim. Acta 91 (2013) 219–226, https://doi.org/10.1016/j.electacta.2012.11.113.
[22] M.N. Garaga, L. Aguilera, N. Yaghini, A. Matic, M. Persson, A. Martinelli, Achieving enhanced ionic mobility in nanoporous silica by controlled surface interactions, PCCP 19 (2017) 5727–5736, https://doi.org/10.1039/c6cp07351d.
[23] P. Vallet, S. Bouzón-Capelo, T. Méndez-Morales, V. Gómez-González, Y. Arosa, R. de la Fuente, E. López-Lago, J.R. Rodríguez, L.J. Gallego, J.J. Parajó, J. Salgado, M. Turmine, L. Segade, O. Cabeza, L.M. Varela, On the physical properties of mixtures of nitrate salts and protic ionic liquids, J. Mol. Liq. 350 (2022) 118483, https://doi.org/10.1016/j.molliq.2022.118483.
[24] J. Salgado, J.J. Parajó, M. Villanueva, J.R. Rodríguez, O. Cabeza, L.M. Varela, Liquid range of ionic liquid – Metal salt mixtures for electrochemical applications, J. Chem. Thermodyn. 134 (2019) 164–174, https://doi.org/10.1016/j.jct.2019.03.012.
[25] J.J. Parajó, P. Vallet, M. Villanueva, Ó. Cabeza, F. Fernández-Carretero, A. García-Luis, M.E. Di Pietro, A. Mele, F. Castiglione, J. Salgado, L.M. Varela, Ionogels based on protic ionic liquid -lithium salt mixtures, J. Mol. Liq. 397 (2024), https://doi.org/10.1016/j.molliq.2024.124093.
[26] V.V. Matveev, A.V. Ievlev, M.A. Vovk, O. Cabeza, J. Salgado-Carballo, J.J. Parajó, J.R. Rodríguez, R. de la Fuente, E. Lähderanta, L.M. Varela, NMR investigation of the structure and single-particle dynamics of inorganic salt solutions in a protic ionic liquid, J. Mol. Liq. 278 (2019) 239–246, https://doi.org/10.1016/j.molliq.2019.01.010.
[27] J.J. Parajó, M. Villanueva, P.B. Sánchez, J. Salgado, Liquid window of some biologically-active ionic liquids, J. Chem. Thermodyn. 126 (2018) 1–10, https://doi.org/10.1016/j.jct.2018.06.014.
[28] H. Weingärtner, NMR studies of ionic liquids: Structure and dynamics, curr opin colloid, Interface Sci. 18 (2013) 183–189, https://doi.org/10.1016/j.cocis.2013.04.001.
[29] L.M. Varela, T. Méndez-Morales, J. Carrete, V. Gómez-González, B. Docampo-Álvarez, L.J. Gallego, O. Cabeza, O. Russina, Solvation of molecular cosolvents and inorganic salts in ionic liquids: A review of molecular dynamics simulations, J. Mol. Liq. 210 (2015) 178–188, https://doi.org/10.1016/j.molliq.2015.06.036.
[30] O. Russina, R. Caminiti, T. Méndez-Morales, J. Carrete, O. Cabeza, L.J. Gallego, L. M. Varela, A. Triolo, How does lithium nitrate dissolve in a protic ionic liquid? J. Mol. Liq. 205 (2015) 16–21, https://doi.org/10.1016/j.molliq.2014.08.007.
[31] H. Zhu, R. Vijayaraghavan, D.R. Macfarlane, M. Forsyth, Self-assembled structure and dynamics of imidazolium-based protic salts in water solution, PCCP 21 (2019) 2691–2696, https://doi.org/10.1039/c8cp07254j.
[32] K. Takao, T. Tsubomura, Weakly-basic anion exchange resin scavenges impurities in ionic liquid synthesized from trialkyloxonium salt, J. Chem. Eng. Data 57 (2012) 2497–2502, https://doi.org/10.1021/je3005003.
[33] P. Charisiadis, V.G. Kontogianni, C.G. Tsiafoulis, A.G. Tzakos, M. Siskos, I. P. Gerothanassis, 1H-NMR as a structural and analytical tool of intra- and intermolecular hydrogen bonds of phenol-containing natural products and model compounds, Molecules 19 (2014) 13643–13682, https://doi.org/10.3390/molecules190913643.
[34] V. Exarchou, A. Troganis, I.P. Gerothanassis, M. Tsimidou, D. Boskou, Do strong intramolecular hydrogen bonds persist in aqueous solution? Variable temperature gradient 1H, 1H–13C GE-HSQC and GE-HMBC NMR studies of flavonols and flavones in organic and aqueous mixtures, Tetrahedron 58 (2002) 7423–7429, https://doi.org/10.1016/S0040-4020(02)00820-7.
[35] M. Hasani, L. Nordstierna, A. Martinelli, Molecular dynamics involving proton exchange of a protic ionic liquid-water mixture studied by NMR spectroscopy, PCCP 21 (2019) 22014–22021, https://doi.org/10.1039/c9cp03563j.
[36] T. Méndez-Morales, J. Carrete, Ó. Cabeza, O. Russina, A. Triolo, L.J. Gallego, L. M. Varela, Solvation of lithium salts in protic ionic liquids: A molecular dynamics study, J. Phys. Chem. B 118 (2014) 761–770, https://doi.org/10.1021/jp410090f.
[37] J. Le Bideau, P. Gaveau, S. Bellayer, M.A. Néouze, A. Vioux, Effect of confinement on ionic liquids dynamics in monolithic silica ionogels: 1H NMR study, PCCP 9 (2007) 5419–5422, https://doi.org/10.1039/b711539c.
[38] J.J. Parajó, M. Villanueva, J. Troncoso, J. Salgado, Thermophysical properties of choline and pyridinium based ionic liquids as advanced materials for energy applications, J. Chem. Thermodyn. 141 (2020) 105947, https://doi.org/10.1016/j.jct.2019.105947.
[39] C.D. Rodríguez Fernández, Y. Arosa, E. López Lago, J. Salgado, P. Verdiá, E. Tojo, O. Cabeza, L.M.L.M. Varela, R. De La Fuente, New insights on the characterization of the ionic liquid crystal 1-ethyl-3-methylimidazolium decylsulfate, J. Phys. Chem. C 123 (2019) 31196–31211, https://doi.org/10.1021/acs.jpcc.9b09660.
[40] H. Ohno, M. Yoshizawa, Ion conductive characteristics of ionic liquids prepared by neutralization of alkylimidazoles, Solid State Ion 154 (2002) 303–309, www.elsevier.com/locate/ssi.
[41] H. Abe, T. Ohkubo, T. Miike, pH variation in protic and pseudo-protic ionic liquid–water solutions, Results Chem. 6 (2023), https://doi.org/10.1016/j.rechem.2023.101045.
[42] J.J. Parajó, P. Vallet, L. Fernández-Miguez, M. Villanueva, O. Cabeza, L.M. Varela, J. Salgado, Thermal Behaviour of Ionogels Based on Ionic Liquid Lithium Salt Mixtures, in: J.A. Seijas (Ed.), Chemistry Proceedings, MDPI, 2020: p. 131. 10.3390/ecsoc-24-08371.
[43] R. Göbel, A. Friedrich, A. Taubert, Tuning the phase behavior of ionic liquids in organically functionalized silica ionogels, Dalton Trans. 39 (2010) 603–611, https://doi.org/10.1039/b913482d.
[44] J.J. Parajó, M. Villanueva, J. Salgado, Thermal stability of ionic liquids, in: J. Seijas, P. Vázquez (Eds.), Ionic Liquids Synthesis, Properties, Technologies and Applications, MDPI, Berlin, 2019, pp. 1–16, https://doi.org/10.1515/9783110583632.
[45] T.J. Wooster, K.M. Johanson, K.J. Fraser, D.R. MacFarlane, J.L. Scott, Thermal degradation of cyano containing ionic liquids, Green Chem. 8 (2006) 691–696, https://doi.org/10.1039/b606395k.
[46] K.J. Baranyai, A.G.B. Deacon, A.D.R. Macfarlane, J.M. Pringle, J.L. Scott, Thermal degradation of ionic liquids at elevated temperatures, Aust. J. Chem. 57 (2004) 145–147.
[47] A. Martinelli, A. Matic, P. Jacobsson, L. Börjesson, A. Fernicola, B. Scrosati, Phase behavior and ionic conductivity in LiTFSI doped ionic liquids of the pyrrolidinium cation and TFSI anion, J. Phys. Chem. B 113 (2009) 11247–11251.
[48] A.J. D'Angelo, M.J. Panzer, Decoupling the ionic conductivity and elastic modulus of gel electrolytes: fully zwitterionic copolymer scaffolds in lithium salt/ionic liquid solutions, Adv. Energy Mater. 8 (2018), https://doi.org/10.1002/aenm.201801646.
[49] B. Lv, G. Zhao, H. Wang, Q. Wang, B. Yang, W. Ma, Z. Li, J. Li, Ionogel fiber-based flexible sensor for friction sensing, Adv. Mater. Technol. 8 (2023), https://doi.org/10.1002/admt.202201617.
[50] A. Guyomard-Lack, J. Abusleme, P. Soudan, B. Lestriez, D. Guyomard, J. Le Bideau, Hybrid silica-polymer ionogel solid electrolyte with tunable properties, Adv. Energy Mater. 4 (2014), https://doi.org/10.1002/aenm.201301570.
[51] R. Sahrash, A. Siddiqa, H. Razzaq, T. Iqbal, S. Qaisar, PVDF based ionogels: applications towards electrochemical devices and membrane separation processes, Heliyon 4 (2018), https://doi.org/10.1016/j.heliyon.2018.e00847.
[52] A. Taubert, R. Löbbicke, B. Kirchner, F. Leroux, First examples of organosilica-based ionogels: Synthesis and electrochemical behavior, Beilstein, J. Nanotechnol. 8 (2017) 736–751, https://doi.org/10.3762/bjnano.8.77.
[53] A. Filippov, O.N. Antzutkin, R. Gimatdinov, O.I. Gnezdilov, Self-diffusion in ionic liquids with nitrate anion: Effects of confinement between glass plates and static magnetic field, J. Mol. Liq. 312 (2020), https://doi.org/10.1016/j.molliq.2020.113404.
[54] J. Leys, M. Wübbenhorst, C. Preethy Menon, R. Rajesh, J. Thoen, C. Glorieux, P. Nockemann, B. Thijs, K. Binnemans, S. Longuemart, Temperature dependence of the electrical conductivity of imidazolium ionic liquids, J. Chem. Phys. 128 (2008) 064509-1–064509-7, https://doi.org/10.1063/1.2827462.
[55] J. Vila, P. Ginés, J.M. Pico, C. Franjo, E. Jiménez, L.M. Varela, O. Cabeza, Temperature dependence of the electrical conductivity in EMIM-based ionic liquids: Evidence of Vogel-Tamman-Fulcher behavior, Fluid Phase Equilib. 242 (2006) 141–146, https://doi.org/10.1016/j.fluid.2006.01.022.
[56] J. Vila, L.M. Varela, O. Cabeza, Cation and anion sizes influence in the temperature dependence of the electrical conductivity in nine imidazolium based ionic liquids, Electrochim. Acta 52 (2007) 7413–7417, https://doi.org/10.1016/j.electacta.2007.06.044.